The Astrophysical Journal, 677:926–942, 2008 April 20

SPITZER UNCOVERS ACTIVE GALACTIC NUCLEI MISSED BY OPTICAL SURVEYS IN SEVEN LATE-TYPE GALAXIES

S. Satyapal,[1] D. Vega,[1] R. P. Dudik,[1,2] N. P. Abel,[3] and T. Heckman[4]

Received 2007 October 9; accepted 2007 December 3

ABSTRACT

We report the discovery using *Spitzer*'s high-resolution spectrograph of seven active galactic nuclei (AGNs) in a sample of 32 late-type galaxies that show no definitive signatures of AGNs in their optical spectra. These observations suggest that the AGN detection rate in late-type galaxies is possibly 4 times larger than what optical spectroscopic observations alone suggest. We demonstrate using photoionization models with an input AGN and an extreme UV–bright starburst ionizing radiation field that the observed mid-infrared line spectrum, which includes the high-ionization [Ne v] 14 μm and/or 24 μm lines, cannot be replicated unless an AGN contribution, in some cases as little as 10% of the total galaxy luminosity, is included. These models show that when the fraction of the total luminosity due to the AGN is low, optical diagnostics are insensitive to the presence of the AGN. In this regime of parameter space, the mid-infrared diagnostics offer a powerful tool for uncovering AGNs missed by optical spectroscopy. The AGN bolometric luminosities in our sample range from $\sim 3 \times 10^{41}$ to $\sim 2 \times 10^{43}$ ergs s^{-1}, which, based on the Eddington limit, corresponds to a lower mass limit for the black hole that ranges from $\sim 3 \times 10^3$ to as high as $\sim 1.5 \times 10^5$ $M_\odot$. These lower mass limits, however, do not put a strain on the well-known relationship between the black hole mass and the host galaxy's stellar velocity dispersion established in predominantly early-type galaxies. Our findings add to the growing evidence that black holes do form and grow in low-bulge environments and that they are significantly more common than optical studies indicate.

Subject headings: black hole physics — dark matter — galaxies: active — galaxies: spiral — infrared: galaxies

Online material: color figures

1. INTRODUCTION

The vast majority of currently known active galactic nuclei (AGNs) in the local universe reside in host galaxies with prominent bulges (e.g., Heckman 1980; Keel 1983; Terlevich et al. 1987; Ho et al. 1997, hereafter H97; Kauffmann et al. 2003). This result, together with the finding that the black hole mass, $M_{\rm BH}$, and the host galaxy's stellar velocity dispersion, σ, are strongly correlated (Gebhardt et al. 2000; Ferrarese & Merritt 2000) has led to the general consensus that black hole formation and growth are fundamentally connected to the buildup of galaxy bulges. Indeed, it has been proposed that feedback from the AGN regulates the surrounding star formation in the host galaxy (e.g., Silk & Rees 1998; Kauffmann & Haehnelt 2000). However, an important outstanding question remains unresolved: *is a bulge in general a necessary ingredient for a black hole to form and grow*? On the one hand, M33, the best-studied nearby bulgeless galaxy, shows no evidence of a supermassive black hole (SMBH), and the upper limit on the mass is significantly below that predicted by the $M_{\rm BH}$-σ relation established in early-type galaxies (Gebhardt et al. 2001; Merritt et al. 2001). On the other hand, both NGC 4395 (Filippenko & Ho 2003) and POX 52 (Barth et al. 2004) show no evidence for a bulge and yet do contain AGNs. However, these two galaxies have remained isolated cases of bulgeless galaxies with accreting black holes, suggesting that they are anomalies. Indeed, in the extensive Palomar optical spectroscopic survey of 486 nearby galaxies (H97), there are only nine optically identified Seyferts with Hubble types of Sc or later. Only one galaxy of Hubble type Scd or later in the entire survey is classified as a Seyfert (NGC 4395). Greene & Ho (2004, 2007) recently conducted an extensive search for broad-line AGNs with intermediate-mass black holes in the Fourth Data Release of the Sloan Digital Sky Survey (SDSS; Greene & Ho 2004, 2007). Of the 8435 broad-line AGNs, they found only 174 (2%) such intermediate-mass objects, indicating that they are extremely rare. Of these, 40% seem to be in late-type galaxies with colors consistent with morphological type Sab, although the SDSS images are of insufficient spatial resolution to extract precise morphological information. Optical observations thus clearly suggest that AGNs in late-type galaxies are uncommon.

However, whether AGNs reside in low-bulge galaxies cannot be definitively determined using optical observations alone. The problem arises because a putative AGN in a galaxy with a minimal bulge is likely to be both energetically weak and deeply embedded in the center of a dusty late-type spiral. As a result, optical emission lines will be dominated by the emission from star formation regions, severely limiting the diagnostic power of optical surveys in determining the incidence of accreting black holes in low-bulge systems. In our previous work, we demonstrated the power of mid-infrared spectroscopy in detecting the low-power AGN in the Sd galaxy NGC 3621 (Satyapal et al. 2007, hereafter S07). AGNs show prominent high-ionization fine-structure line emission at mid-infrared wavelengths, but starburst and normal galaxies are characterized by lower ionization spectra characteristic of H II regions ionized by young stars (e.g., Genzel et al. 1998; Sturm et al. 2002; Satyapal et al. 2004). In particular, the [Ne v] 14 μm (ionization potential 97 eV) line is not generally produced in H II regions surrounding young stars, the dominant energy source in starburst galaxies, since even hot massive stars emit very few photons with energy sufficient for the production of Ne^{4+}. The detection of this line in any galaxy provides strong evidence for an AGN.

[1] Department of Physics and Astronomy, George Mason University, 4400 University Drive, MS 3F3, Fairfax, VA 22030; satyapal@physics.gmu.edu.
[2] Observational Cosmology Laboratory, NASA Goddard Space Flight Center, Greenbelt, MD 20711.
[3] Department of Physics, University of Cincinnati, Cincinnati, OH 45221.
[4] Center for Astrophysical Sciences, Department of Physics and Astronomy, The Johns Hopkins University, Baltimore, MD 21218.

TABLE 1
PROPERTIES OF THE SAMPLE

Galaxy Name (1)	Distance (Mpc) (2)	Hubble Type (3)	T (4)	$M^0_{B_T}$ (5)	[O III]/Hβ (6)	[O I]/Hα (7)	[N II]/Hα (8)	[S II]/Hα (9)	Optical Class (10)
NGC 925	9.4	SAB(s)d	7	−19.90	0.84	0.01	0.22	0.33	H
NGC 1569	1.6	IBm	10	−16.60	5.48	0.00	0.04	0.03	H
NGC 2276	36.8	SAB(rs)c	5	−21.08	0.15	0.01	0.35	0.18	H
NGC 2903	6.3	SAB(rs)bc	4	−19.89	0.10	0.01	0.34	0.19	H
NGC 2976	2.1	SAc pec	5	−16.31	1.42	0.01	0.31	0.18	H
NGC 3034	5.2	IAO spin	90	−19.72	0.36	0.01	0.56	0.18	H
NGC 3077	2.1	IAO pec	90	−16.29	0.75	0.00	0.21	0.15	H
NGC 3184	8.7	SAB(rs)cd	6	−19.36	0.13	0.01	0.33	0.20	H
NGC 3198	10.8	SB(rs)c	5	−19.96	0.23	0.03	0.42	0.32	H
NGC 3310	18.7	SAB(r)bc pec	4	−20.41	0.95	0.04	0.66	0.26	H
NGC 3367	43.6	SB(rs)c	5	−21.28	0.50	0.03	0.83	0.28	H
NGC 3556	14.1	SB(s)cd spin	6	−20.92	0.26	0.01	0.32	0.29	H
NGC 3726	17.0	SAB(r)c	5	−20.48	0.14	0.01	0.31	0.22	H
NGC 3938	17.0	SA(s)c	5	−20.32	1.76	0.14	0.53	1.67	H
NGC 3949	17.0	SA(s)bc	4	−20.01	0.22	0.05	0.40	0.44	H
NGC 4088	17.0	SAB(rs)bc	4	−20.63	0.21	0.01	0.32	0.18	H
NGC 4192	17.0	SA(s)cd spin	6	−19.52	1.87	0.14	1.41	1.02	T2
NGC 4214	3.5	IAB(s)m	H	−17.58	3.67	0.01	0.07	0.13	H
NGC 4236	2.2	SB(s)dm	8	−17.18	2.04	0.03	0.17	0.44	H
NGC 4254	16.8	SA(s)c	5	−21.03	0.90	0.02	0.48	0.23	H
NGC 4273	35.1	SB(s)c	5	−20.68	0.18	0.01	0.38	0.23	H
NGC 4321	16.8	SAB(s)bc	4	−21.15	0.79	0.11	1.18	0.48	T2
NGC 4414	9.7	SA(rs)c	5	−19.31	0.58	0.14	0.59	0.50	T2
NGC 4490	7.8	SB(s)d pec	7	−19.65	2.55	0.12	0.25	0.71	H
NGC 4536	13.3	SAB(rs)bc	4	−20.04	0.33	0.03	0.47	0.36	H
NGC 4559	9.7	SAB(rs)cd	6	−20.17	0.35	0.03	0.42	0.40	H
NGC 4567	16.8	SA(rs)bc	4	−19.34	0.12	0.02	0.28	0.16	H
NGC 4631	6.9	SB(s)d spin	7	−20.58	1.53	0.03	0.24	0.23	H
NGC 5055	7.2	SA(rs)bc	4	−20.26	1.85	0.17	1.48	0.74	T2
NGC 5474	6.0	SA(s)cd pec	6	−17.59	1.76	0.02	0.14	0.27	H
NGC 5907	14.9	SA(s)c spin	5	−21.17	1.07	0.03	0.60	0.34	H
NGC 6946	5.5	SAB(rs)cd	6	−20.92	0.38	0.04	0.64	0.32	H
IC 342	3.0	SAB(rs)cd	6	−21.35	0.10	0.01	0.45	0.22	H

NOTES.—Col. (1): Common source names. Col. (2): Distance to the source in units of Mpc taken directly from H97, where distances for objects closer than 40 Mpc were adopted from Tully & Shaya (1984) and those farther than 40 Mpc were obtained using systemic velocities and assuming $H_0 = 75$ km s^{-1} Mpc^{-1}. Col. (3): Hubble type. Col. (4): Numerical Hubble type index as listed in H97. Col. (5): Total absolute B magnitude corrected for extinction, adopted from H97. Col. (6): [O III]-to-Hβ ratio taken from H97. Col. (7): [O I]-to-Hα ratio taken from H97. Col. (8): [N II]-to-Hα ratio taken from H97. Col. (9): [S II]-to-Hα ratio taken from H97. Col. (10): Optical classification of the source; "H" signifies H II region ratios, "T" represents transitional spectra between LINERs and H II regions, and "2" indicates that broad permitted lines were not found in the optical spectrum.

The goal of this paper is to answer the question, are AGNs in late-type galaxies more common than previously thought? If so, this would revise our understanding of the environments in which SMBHs can form and grow and perhaps shed light on the nature of the $M_{\rm BH}$-σ relation in low-bulge systems. Toward this end, we conducted an archival investigation of 32 late-type galaxies observed by the *Spitzer* high-resolution spectrograph that show no definitive optical signatures of AGNs to search for low-power and/or deeply embedded AGNs.

This paper is structured as follows. In § 2 we summarize the properties of the *Spitzer* archival sample presented in this paper. In § 3 we summarize the observational details and data analysis procedures, followed by a description of our results in § 4. In § 5 we discuss the origin of the [Ne V] emission, with each galaxy discussed individually, followed by a discussion of the implications of our discoveries in § 6. A summary of our major conclusions is given in § 7.

2. THE SAMPLE

The target sources were selected from the Palomar survey of nearby bright galaxies (H97). Of the 486 galaxies in the Palomar survey, 169 are of Hubble type Sbc or later and classified based on their optical line ratios as "H II" stellar-powered galaxies or "T2" transition galaxies. T2 galaxies have optical line ratios intermediate between those of H II galaxies and low-ionization nuclear emission-line regions (LINERs) and have no broad permitted lines (e.g., Hα) in their optical spectra. Therefore, there is no firm optical spectroscopic evidence for AGNs in these galaxies. Of these 169 galaxies, 32 were observed by the high-resolution modules of the Infrared Spectrograph (IRS; Houck et al. 2004) on board *Spitzer*.

Table 1 summarizes the basic properties of the galaxies in our sample. All targets are nearby, ranging in distance from 1.6 to 43.6 Mpc. The majority of galaxies are classified as H II galaxies; only 4 out of 32 are T2 objects. Figure 1 shows the distribution of Hubble types for the sample. Note that there are only two Sd galaxies and one Sdm galaxy in the sample and that the majority of galaxies are of Hubble types Sc and Sbc.

Figure 2 shows the standard optical line ratio diagnostic diagrams (Veilleux & Osterbrock 1987) widely used to classify AGNs for the entire H97 sample, with our *Spitzer* sample highlighted. We also show in Figure 2 the theoretical starburst limit line from

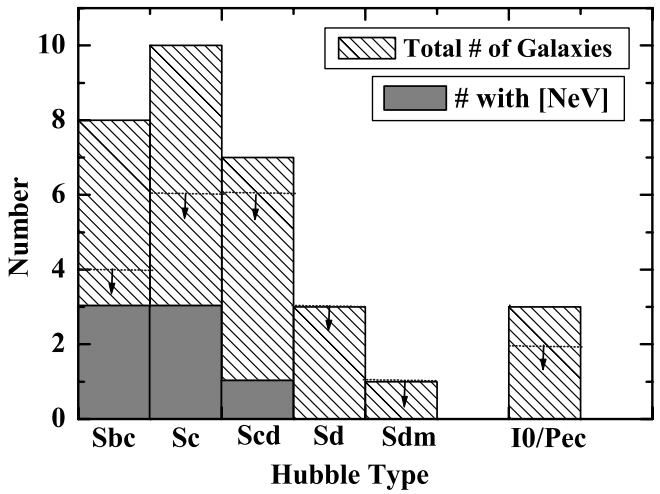

FIG. 1.—Distribution of Hubble types for the sample. The galaxies with [Ne v] detections are indicated by the filled histogram (see § 4 for details). Since the sensitivity of the observations varied across the sample, we also indicate with arrows the number of galaxies with [Ne v] 14 μm line sensitivity of 10^{38} ergs s^{-1} or better. Although the sample size is too small to make statistically meaningful statements, we note that none of the galaxies of Hubble type later than Scd in this sample display a [Ne v] line. [*See the electronic edition of the Journal for a color version of this figure*.]

Kewley et al. (2001). This line represents the maximum line ratios possible from starburst photoionization models using the hardest possible starburst input ionizing radiation field. Note that the majority of galaxies in our sample (~85%–94%, depending on the diagram) have optical line ratios well to the left of this line, indicating that the optical line ratios do not require the presence of *any* AGN contribution. We point out that the optical spectroscopic classification of a galaxy, in principle, will depend on the measurement aperture size, particularly in sources with weak AGNs surrounded by vigorous star formation activity. However, the aperture size employed in the H97 optical spectral measurements ($\sim 2'' \times 4''$) is in general one of the smallest available in the literature. In addition, the sensitivity of the observations is considerably higher relative to many other surveys; therefore, the optical line ratios from H97 provide the most sensitive optical classifications for weak AGNs currently available.

3. OBSERVATIONAL DETAILS AND DATA REDUCTION

All data presented in this work were obtained using both the short-wavelength (SH; $4.7'' \times 11.3''$, $\lambda = 9.9$–19.6 μm) and long-wavelength (LH; $11.1'' \times 22.3''$, $\lambda = 18.7$–37.2 μm) high-resolution modules of the IRS. These modules have a spectral resolution of $R \sim 600$. The 32 observations were archived from various programs, including the SINGS Legacy Program (Kennicutt et al. 2003), and therefore contain both spectral mapping and staring observations. In spectral mapping mode, the

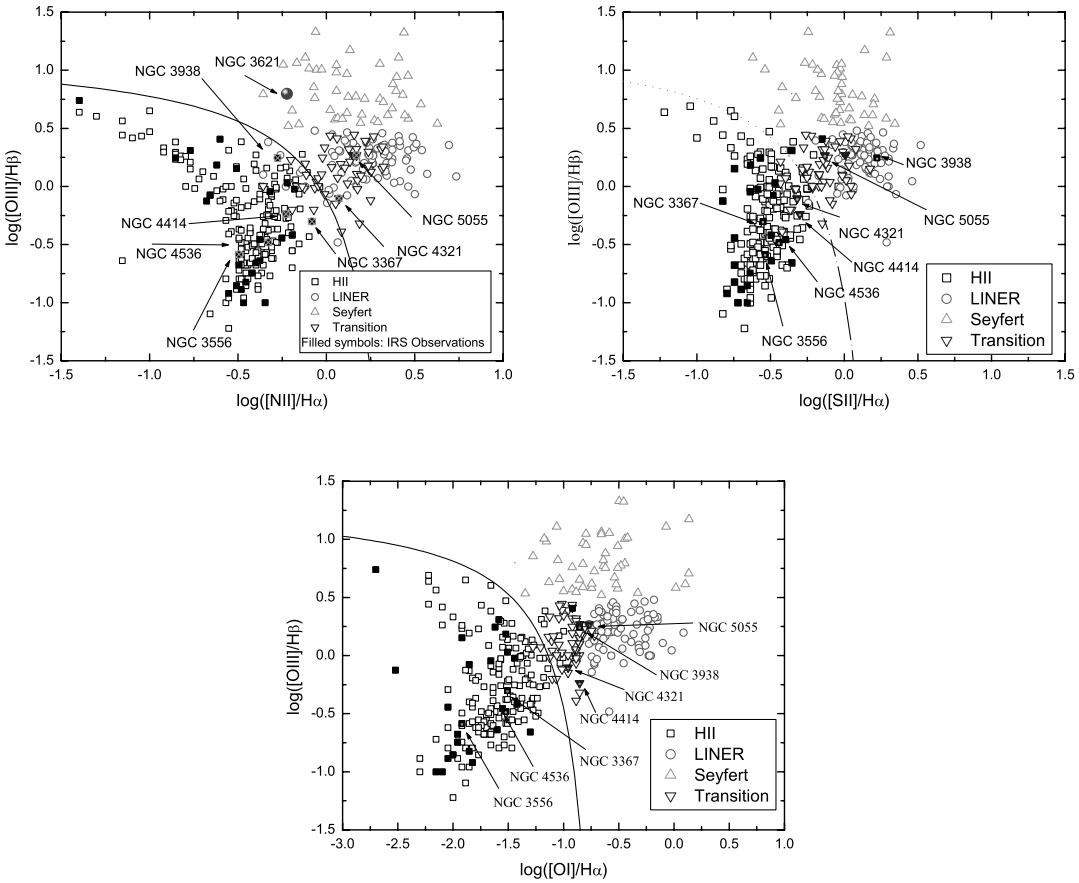

FIG. 2.—Standard optical line ratio diagnostic diagrams (Veilleux & Osterbrock 1987) widely used to classify AGNs for the entire H97 sample, with our *Spitzer* sample represented by the filled symbols. The solid line represents the theoretical starburst limit line from Kewley et al. (2001). This line represents the maximum line ratios possible from purely starburst photoionization models. The galaxies with [Ne v] detections are labeled in the figure (see § 4 for details). Note that most of the galaxies with [Ne v] detections are to the left of the starburst limit line, indicating that their optical line ratios are purely consistent with star formation. [*See the electronic edition of the Journal for a color version of this figure*.]

TABLE 2
Observational Details

Galaxy Name (1)	PID (2)	Instrument Mode (3)	Exposure Time SH (4)	Exposure Time LH (5)	Position (J2000.0) R.A. (6)	Position (J2000.0) Decl. (7)	Extraction Aperture Size SH (8)	Extraction Aperture Size LH (9)
NGC 925	159	Mapping	60	60	02 27 16.90	+33 34 45.00	14 × 25	14 × 25
NGC 1569	117	Mapping	600	1200	04 30 49.10	+64 50 53.00	5 × 57	22 × 33
NGC 2276	20140	Staring	60	120	07 27 14.30	+85 45 16.00	5 × 11	11 × 22
NGC 2903	59	Staring	120	120	09 32 10.10	+21 30 04.00	5 × 11	11 × 22
NGC 2976	159	Mapping	60	60	09 47 15.40	+67 54 59.00	14 × 25	14 × 25
NGC 3034	21	Mapping	24	30	09 55 52.20	+69 40 47.00	27 × 27	27 × 27
NGC 3077	73	Staring	30	14	10 03 19.10	+68 44 02.00	5 × 11	11 × 22
NGC 3184	159	Mapping	60	60	10 18 17.00	+41 25 28.00	14 × 25	14 × 25
NGC 3310	14	Staring	120	120	10 38 45.96	+53 30 05.30	5 × 11	11 × 22
NGC 3367	59	Staring	240	120	10 46 34.96	+13 45 02.80	5 × 11	11 × 22
NGC 3198	159	Mapping	60	60	10 19 55.05	+45 32 59.50	14 × 25	14 × 25
NGC 3556	14	Staring	120	120	11 11 30.97	+55 40 26.80	5 × 11	11 × 22
NGC 3726	3124	Staring	240	240	11 33 21.17	+47 01 44.70	5 × 11	11 × 22
NGC 3938	159	Mapping	60	60	11 52 50.30	+44 07 15.00	5 × 11	11 × 22
NGC 3949	3124	Staring	240	240	11 53 41.74	+47 51 31.50	5 × 11	11 × 22
NGC 4088	14	Staring	120	120	12 05 34.19	+50 32 20.50	5 × 11	11 × 22
NGC 4192	3237	Staring	480	300	12 13 48.29	+14 54 01.20	5 × 11	11 × 22
NGC 4236	159	Mapping	60	60	12 16 42.10	+69 27 45.00	14 × 25	14 × 25
NGC 4273	20140	Staring	60	120	12 19 56.10	+05 20 35.00	5 × 11	11 × 22
NGC 4254	159	Mapping	60	60	12 18 49.60	+14 24 59.00	14 × 25	14 × 25
NGC 4321	159	Mapping	60	60	12 22 54.93	+15 49 21.80	27 × 43	31 × 49
NGC 4490	3124	Staring	240	240	12 30 36.37	+41 38 37.10	5 × 11	11 × 22
NGC 4414	3674	Staring	240	180	12 26 27.10	+31 13 24.70	5 × 11	11 × 22
NGC 4536	159	Mapping	60	60	12 34 27.35	+02 11 25.50	9 × 9	9 × 9
NGC 4559	159	Mapping	60	60	12 35 57.70	+27 57 35.00	14 × 25	14 × 25
NGC 4567	20140	Staring	60	120	12 36 32.80	+11 15 26.00	5 × 11	11 × 22
NGC 4631	159	Mapping	60	60	12 42 08.01	+32 32 29.40	16 × 25	16 × 25
NGC 5055	159	Mapping	60	60	13 15 49.30	+42 01 52.00	5 × 11	11 × 22
NGC 5474	159	Mapping	60	60	14 05 01.61	+53 39 44.00	14 × 25	14 × 25
NGC 5907	3124	Staring	240	240	15 15 53.69	+56 19 43.90	5 × 11	11 × 22
NGC 6946	159	Mapping	60	60	20 34 52.30	+60 09 14.00	18 × 31	18 × 31
IC 342	14	Staring	120	112	03 46 48.51	+68 05 46.00	5 × 11	11 × 22

Notes.—Col. (1): Common source names. Col. (2): Project identification number. Col. (3): Instrument mode for the observation. Cols. (4) and (5): Exposure time per pointing in seconds given for the SH and LH modules, respectively. Cols. (6) and (7): Position of peak flux of [Ne v] 14 μm when detected and 2MASS or radio nuclear coordinates otherwise. Units of right ascension are hours, minutes, and seconds, and units of declination are degrees, arcminutes, and arcseconds. Cols. (8) and (9): Extraction apertures for mapping observations could be matched using CUBISM, whereas single slit sizes are quoted for staring observations. Values given are in arcseconds.

spacecraft moves in a raster pattern of discrete steps, generally of half-slit width and half-slit length in size, in order to construct a rectangular map of the targeted region. The SH and LH maps for the observations vary in size. In Table 2 we summarize the observational details for our sample. The apertures from which our fluxes were extracted are listed in Table 2 and correspond to either the size of a single slit if the galaxy was observed as a staring observation or the maximum overlap aperture between the SH and LH maps such that both the SH and LH spectra correspond to the same physical region on the sky. For the SINGS observations, this corresponds to roughly a $23'' \times 15''$ aperture. In some mapping observations, the [Ne v] line was detected in a small aperture, but not in the largest possible extraction region. In these cases, the aperture used to obtain the [Ne v] detection is listed in Table 2. Here, identical apertures for both the SH and LH modules were also used so that spectra from both modules corresponded to the same physical region.

The data presented here were preprocessed by the IRS pipeline (ver. 15.3) at the *Spitzer* Science Center prior to download. Preprocessing includes ramp fitting, dark-sky subtraction, droop correction, linearity correction, flat-fielding, and flux calibration.[5] For all mapping observations we used the pipeline-processed "BCD-level" data products downloaded from the *Spitzer* archive in conjunction with CUBISM version 1.5[6] (Kennicutt et al. 2003; Smith et al. 2004) to construct the high-resolution spectral cubes. The two-dimensional FITS output images from CUBISM were smoothed using a Gaussian kernel of 1.5 pixels in width. To extract final one-dimensional spectra and line maps, we used the `cubeview` and `cubespec` tools within CUBISM. Detailed descriptions of the postprocessing steps included in CUBISM are given in Smith et al. (2004). The *Spitzer* spectra obtained from both staring and mapping observations were further processed using the SMART version 6.2.4 analysis package (Higdon et al. 2004) and the corresponding version of the calibration files (ver. 1.4.8), which were used to obtain final line fluxes.

All of the staring observations were centered on the nucleus of the galaxy, as requested, and generally corresponded to the

[5] See *Spitzer* Observers Manual, chapter 7, http://ssc.spitzer.caltech.edu/documents/som/som8.0.irs.pdf.

[6] Available at http://ssc.spitzer.caltech.edu/archanaly/contributed/cubism/index.html.

2MASS nuclear coordinates. We note that the SH and LH staring observations included data from two slit positions overlapping by one-third of a slit. Because the slits occupied distinctly different regions of the sky, the flux from the slits could not be averaged unless the emission originated from a compact source that was contained entirely in each slit. Therefore, the procedure for flux extraction for staring observations was as follows: (1) If the fluxes measured from the two slits differed by no more than the calibration error of the instrument, then the fluxes were averaged; otherwise, the slit with the highest measured line flux was chosen. (2) If an emission line was detected in one slit, but not in the other, then the detection was selected. The slit for the SH and LH modules was too small for background subtraction to take place, and separate SH or LH background observations did not exist for any of the galaxies in this sample. We therefore did not perform any background subtraction on any of the observations presented in this work. The overall calibration uncertainty for the fluxes we report in this paper is 25%–30% for all mapping observations and 15% for staring observations.

4. RESULTS

4.1. *Line Fluxes and Spectral Line Fits*

In Table 3 we list the line fluxes, statistical errors, and upper limits for the SH and LH observations for the [Ne v] 14.3 and 24.3 μm lines, as well as the 26 μm [O iv] line. The apertures from which these fluxes were extracted are listed in Table 2. In all cases, detections were defined when the line flux was at least 3 σ. We detected either the [Ne v] 14.3 or 24.3 μm line in 7 out of the 32 galaxies, providing strong evidence for the presence of an AGN in these galaxies. The [O iv] 26 μm line (ionization potential = 55 eV) was detected in 12 out of the 32 galaxies. Although this line is generally strong in powerful AGNs (e.g., Genzel et al. 1998; Sturm et al. 2002), it can be produced purely by photoionization by very hot stars or shock-heated gas (Schaerer & Stasińska 1999) and is therefore not a definitive signature of an AGN. The spectral line fits for the detected [Ne v] lines, as well as the [O iv] 26 μm and [Ne iii] 15.5 μm lines, when detected, for each of the seven galaxies are shown in Figure 3. We note that the spectral resolution of the SH and LH modules of the IRS is insufficient to resolve the velocity structure for most of the lines.

The optical line ratios of the galaxies with [Ne v] detections are shown in Figure 1. As can be seen, several of the galaxies with [Ne v] detections lie significantly to the left of the theoretical-limit line from Kewley et al. (2001), indicating that there is no hint of the presence of an AGN from the optical emission lines alone. Three out of the seven galaxies with [Ne v] detections are classified by H97 as transition objects, as can be seen in Table 1. The [Ne v] 14.3 or 24.3 μm line was not detected in only one out of the total of four transition objects in our sample of 32 galaxies.

4.2. *Infrared Emission-Line Morphologies*

The signal-to-noise ratio of the observations was insufficient to provide detailed spatial information on the [Ne v] emission for all four of the AGN candidates with mapping observations. However, in Figure 4 we show the detected [O iv] 26 μm and [Ne iii] 15.5 μm images for three out of the four galaxies with [Ne v] detections. The signal-to-noise ratio corresponding to both the [O iv] and the [Ne iii] for NGC 3968 precluded any analysis of the spatial distribution of the emission in this galaxy. This galaxy is therefore excluded from Figure 4. The ionization potentials of O iv and Ne iii are 55 and 41 eV, respectively. Both species can be produced in gas ionized by hot stars. However, in all cases, centrally compact emission is observed, suggestive of an AGN origin. Although we do not know the spatial morphology of the [Ne v] emission, it is likely to be similar to that of the centrally concentrated [O iv] and [Ne iii] emission shown below. We note that there is possibly one anomalous galaxy in our sample of detections. The peak of the [Ne v] emission in NGC 4536 appears to be offset from the peak of the [O iv] and [Ne iii] emission, which both peak at the optical and 2MASS nucleus. However, the signal-to-noise ratio of the data severely hampers any detailed study of the spatial distribution of the [Ne v] emission in this galaxy (see § 5.1 for details). We discuss each galaxy individually in § 5.1.

TABLE 3
Fluxes for Full Sample

Galaxy Name (1)	[Ne v] 14.32 μm (97.1 eV) (2)	[Ne v] 24.32 μm (97.1 eV) (3)	[O iv] 25.89 μm (54.9 eV) (4)
NGC 925	<1.0	<0.48	0.63 ± 0.19
NGC 1569	<0.15	<1.0	25.0 ± 6.6
NGC 2276	<0.56	<0.39	<0.69
NGC 2903	<0.47	<2.7	<4.0
NGC 2976	<0.81	<0.37	<0.28
NGC 3034	<111.1	<250.6	<259.6
NGC 3077	<0.45	<0.75	<0.81
NGC 3184	<0.70	<0.59	0.57 ± 0.17
NGC 3310	<0.38	<1.7	3.9 ± 0.8
NGC 3367	1.2 ± 0.3	0.93 ± 0.24	0.81 ± 0.23
NGC 3198	<0.80	<0.93	<0.82
NGC 3556	0.40 ± 0.09	<1.1	<1.5
NGC 3726	<0.30	<0.66	<0.62
NGC 3938	<4.43	1.1 ± 0.3	0.56 ± 0.19
NGC 3949	<0.31	<0.54	0.92 ± 0.29
NGC 4088	<0.39	<0.68	<0.73
NGC 4192	<0.59	<1.5	<1.2
NGC 4236	<0.85	<0.45	<0.41
NGC 4273	<0.62	<0.40	<1.28
NGC 4254	<0.90	<0.41	1.6 ± 0.5
NGC 4321	2.6 ± 0.8	<3.6	<5.6
NGC 4490	<0.22	<0.46	1.3 ± 0.2
NGC 4414	<0.65	1.2 ± 0.4	2.1 ± 0.3
NGC 4536	0.32 ± 0.09	<0.90	<1.2
NGC 4559	<0.84	<0.39	<0.40
NGC 4567	<0.53	<0.45	<0.54
NGC 4631	<2.0	<1.35	<4.7
NGC 5055	0.56 ± 0.18	<0.55	1.4 ± 0.2
NGC 5474	<1.1	<0.44	<0.32
NGC 5907	<0.23	<0.58	1.3 ± 0.2
NGC 6946	<1.5	<0.39	<12.07
IC 342	<1.7	<15.88	<23.37

Notes.—Col. (1): Common source names. Cols. (2)–(4): Fluxes are in units of 10^{-21} W cm^{-2}; 3 σ upper limits are reported for nondetections.

4.3. *Line Flux Ratios and Luminosities*

Since the ratio of high- to low-excitation lines depends on the nature of the ionizing source, the [Ne v] 14 μm/[Ne ii] 12.8 μm and the [O iv] 25.9 μm/[Ne ii] 12.8 μm line flux ratios have been used to characterize the nature of the dominant ionizing source in galaxies (Genzel et al. 1998; Sturm et al. 2002; Satyapal et al. 2004; Dale et al. 2006). Table 4 lists the [Ne v]/[Ne ii], [Ne v]/[Ne iii], and [O iv]/[Ne ii] line flux ratios and the [Ne v] 14.3 μm line luminosities for the seven galaxies in which either [Ne v] line is detected. In NGC 3938 and NGC 4414 the [Ne v] 14.3 μm line was not detected. In this case we estimated and use in Table 4 the

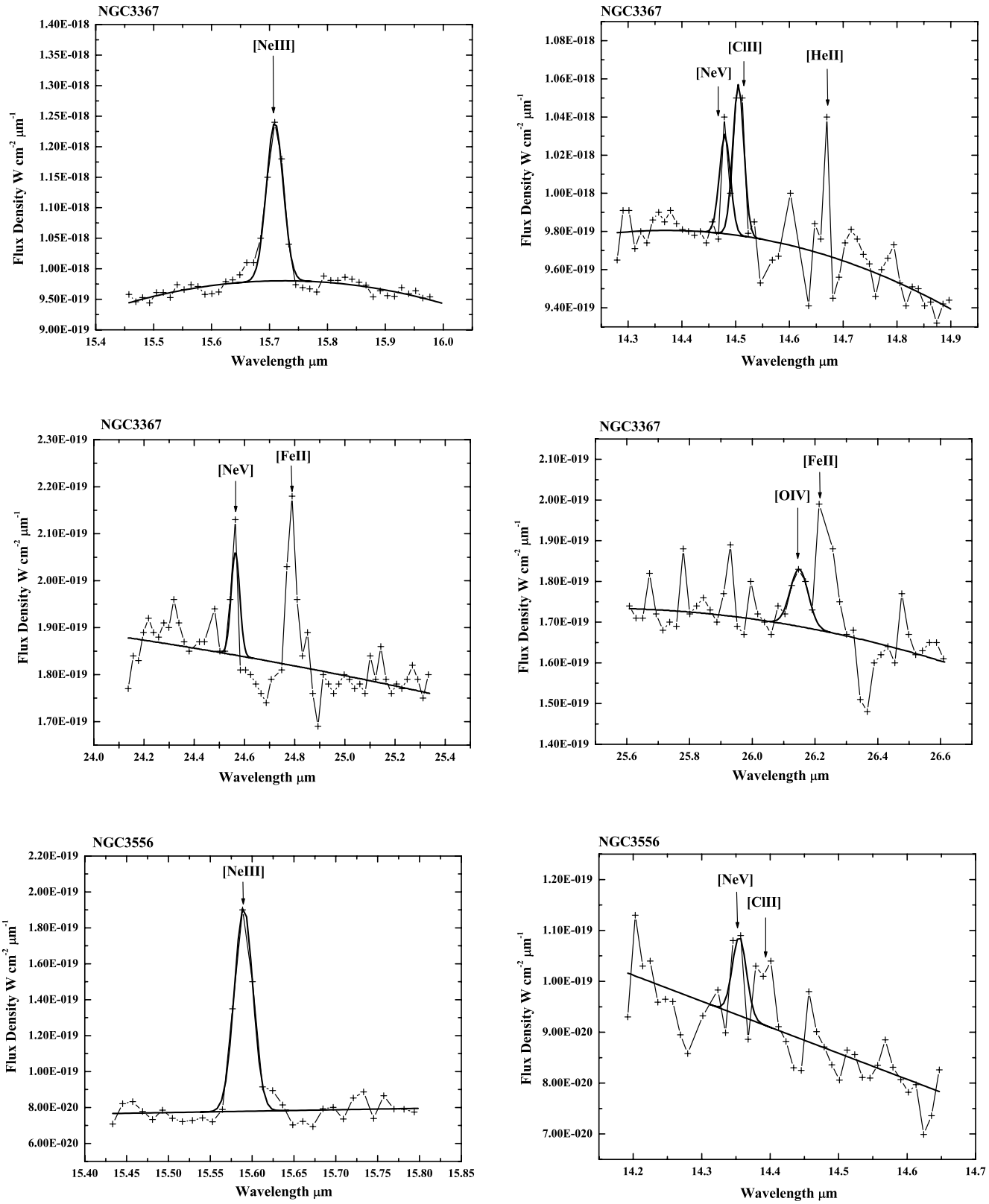

FIG. 3.—IRS spectra showing the detections of the [Ne V] 14.3 μm and /or [Ne V] 24.3 μm line for the seven galaxies with detections listed in Table 4. Also shown are spectra showing the [Ne III] 15.5 μm and [O IV] 26 μm lines when detected for each of the galaxies.

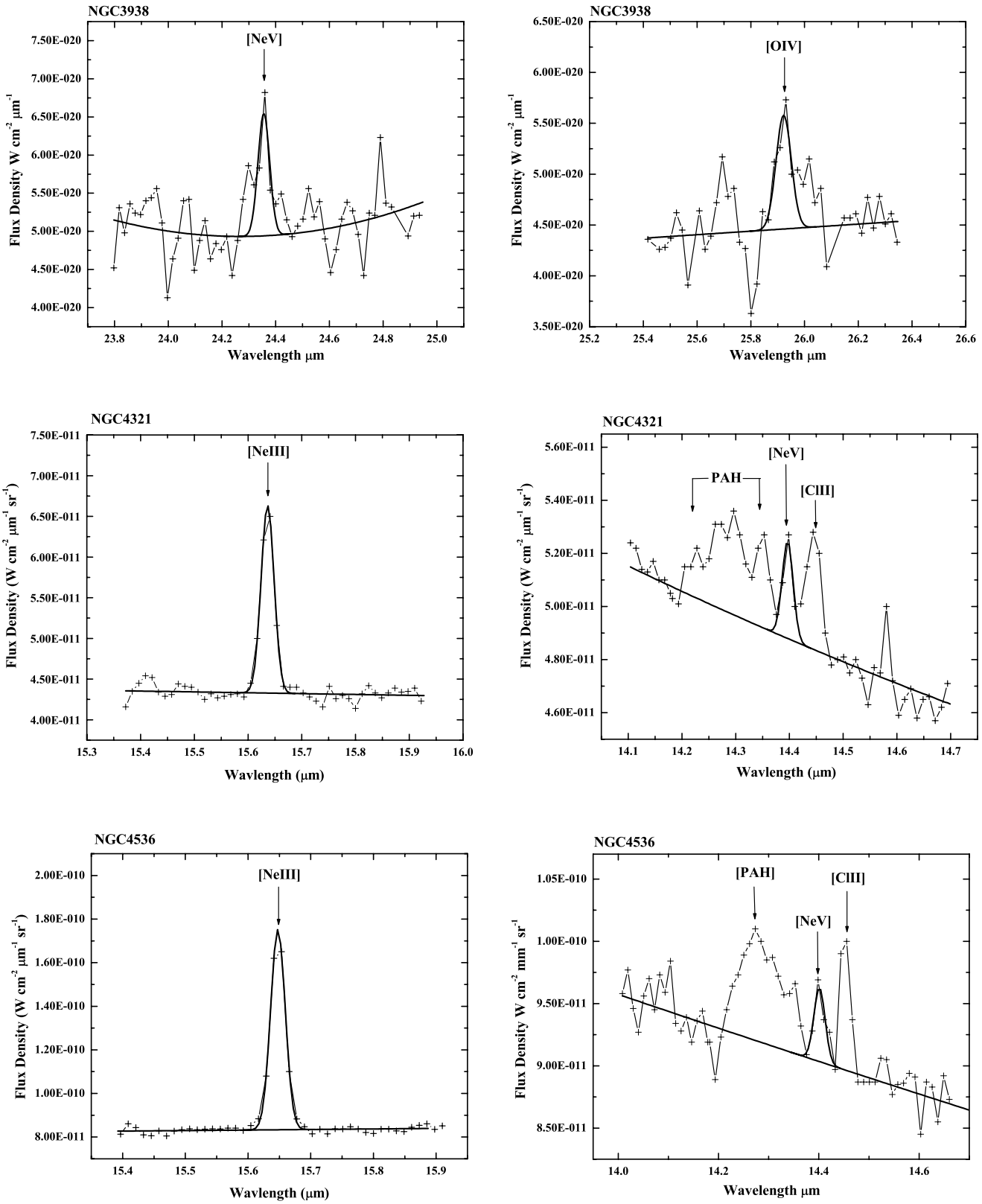

FIG. 3—*Continued*

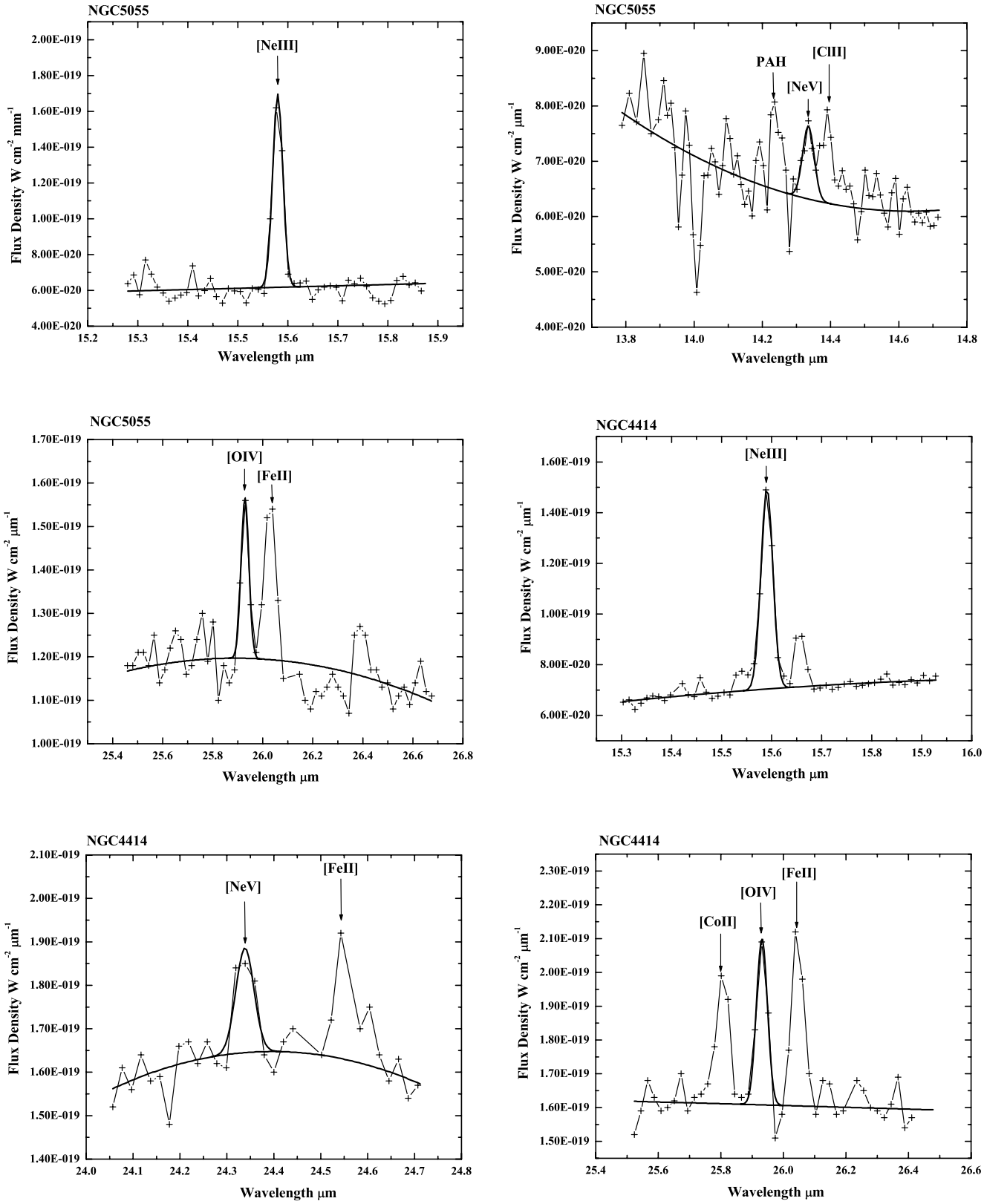

FIG. 3—*Continued*

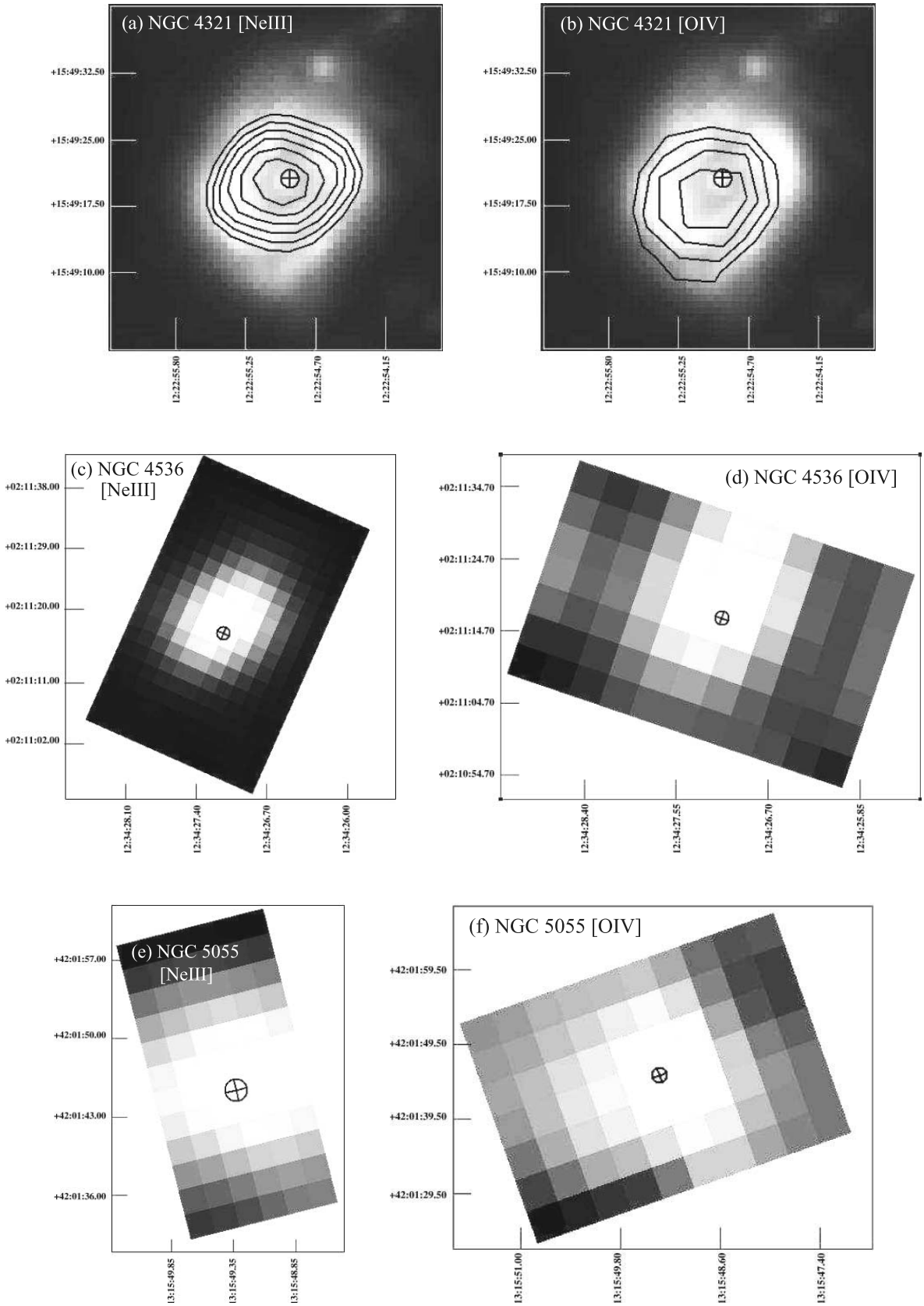

FIG. 4.—(*a*) [Ne III] 15.5 μm continuum-subtracted image of NGC 4321. Contour overlays of the archival IRAC 8 μm image are also shown and display the prominent circumnuclear star formation ring in this galaxy. Note that there are two components to the [Ne III] emission: one that follows the circumnuclear ring and a compact centrally concentrated component likely originated from gas ionized by the AGN. (*b*) [O IV] 26 μm continuum-subtracted image of NGC 4321 with contour overlays of the [Ne II] 12.8 μm emission. Note that the [Ne II] emission traces the circumnuclear ring but the [O IV] emission is compact and centrally concentrated, which is highly suggestive of an AGN origin. (*c*) [Ne III] 15.5 μm continuum-subtracted image of NGC 4536. (*d*) [O IV] 26 μm continuum-subtracted image of NGC 4536. The emission appears to be associated with the nucleus; however, the [Ne V] emission seems to be offset from the nuclear coordinates. See § 5.1 for details. (*e*) [Ne III] 15.5 μm continuum-subtracted image of NGC 5055. (*f*) [O IV] 26 μm continuum-subtracted image of NGC 5055. The cross in each panel indicates the nuclear coordinates from the 2MASS database. Note that in all images the emission is concentrated and centered on the nucleus, suggesting an AGN as the ionizing source.

TABLE 4

LINE RATIOS AND LUMINOSITIES OF AGN CANDIDATE GALAXIES

Galaxy Name (1)	Projected Aperture Size SH (kpc) (2)	Projected Aperture Size LH (kpc) (3)	[Ne v] 14.32 μm/[Ne ii] 12.81 μm (4)	[Ne v] 14.32 μm/[Ne iii] 15.56 μm (5)	[O iv] 25.89 μm/[Ne ii] 12.81 μm (6)	L[Ne v] 14.32 μm (7)
NGC 3367	0.99 × 2.4	2.3 × 4.7	0.010 ± 0.003	0.117 ± 0.035	0.007 ± 0.002	39.415
NGC 3556	0.32 × 0.77	0.76 × 1.5	0.017 ± 0.004	0.126 ± 0.030	<0.063	37.950
NGC 3938[a]	0.39 × 0.93	0.91 × 1.8	0.457 ± 0.149	>0.053	0.314 ± 0.113	38.426
NGC 4321	2.2 × 3.5	2.5 × 4.0	0.016 ± 0.005	0.134 ± 0.041	<0.035	38.913
NGC 4414[a]	0.22 × 0.53	0.52 × 1.0	0.154 ± 0.048	0.391 ± 0.123	0.361 ± 0.050	37.980
NGC 4536[b]	0.58 × 0.58	0.58 × 0.58	0.012 ± 0.003	0.062 ± 0.017	<0.047	37.803
NGC 5055	0.16 × 0.39	0.39 × 0.78	0.108 ± 0.035	0.206 ± 0.068	0.279 ± 0.041	37.516

NOTES.—Col. (1): Common source names. Col. (2): Dimensions of the extraction region from the SH observation. Col. (3): Dimensions of the extraction region from the LH observation. Col. (4): Ratio of flux of [Ne v] 14.32 μm to [Ne ii] 12.81 μm; uncertainties reported in cols. (4)–(6) are based on calibration uncertainties on the line flux of 30% for mapping observations and 15% for staring. Col. (5): Ratio of flux of [Ne v] 14.32 μm to [Ne iii] 15.56 μm. Col. (6): Ratio of flux of [O iv] 25.89 μm to [Ne ii] 12.81 μm; upper limits provided for nondetections based on 3 σ upper limit for [O iv]. Col. (7): Log of luminosity of [Ne v] 14.32 μm in units of ergs s^{-1}.

[a] Flux of [Ne v] 14.32 μm estimated using [Ne v] 24.32 μm flux, according to eq. (1); see § 4.3.

[b] [Ne v] 14.32 μm emitting region does not overlap with 2MASS nuclear coordinates. See Table 2 for exact coordinates.

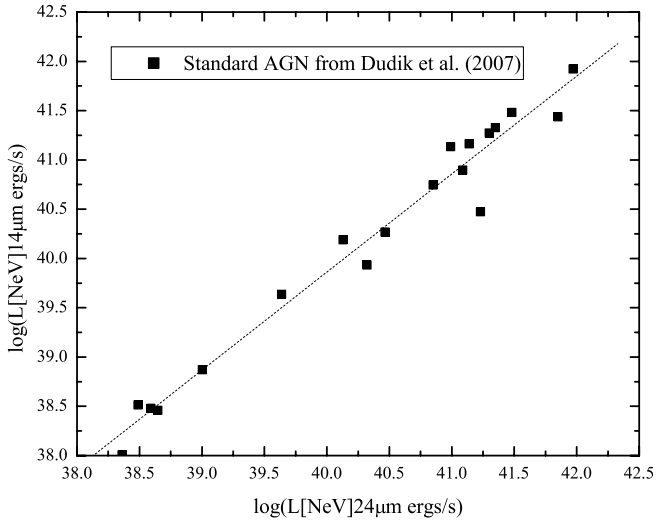

FIG. 5.—[Ne v] 14.3 μm line luminosity as a function of the [Ne v] 24.3 μm line luminosity in known AGNs that currently have [Ne v] observations (Dudik et al. 2007). The figure clearly shows a strong correlation. The Spearman rank correlation coefficient between the 14.3 and 24.3 μm line luminosities is $r_S = 0.97$, with a probability of chance correlation of 6.7×10^{-12}, indicating a significant correlation. The rms scatter in the relation is 0.219 dex.

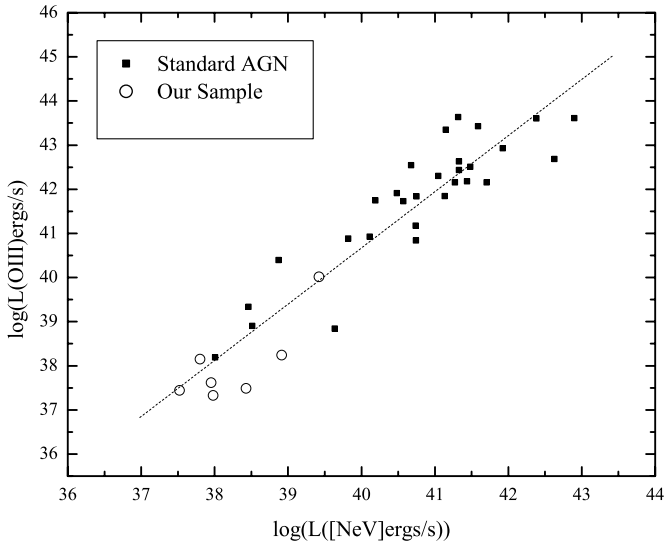

FIG. 6.—[O III] λ5007 line luminosity vs. the [Ne v] 14.3 μm line luminosity for standard optically identified AGNs and our sample of galaxies. There is a significant correlation between the luminosities. The Spearman rank correlation coefficient between the line luminosities is $r_S = 0.84$, with a probability of chance correlation of 8×10^{-6}, indicating a significant correlation. The rms scatter in the relation is 0.67 dex.

14.3 μm line luminosity using the [Ne v] 24.3 μm line luminosity. The [Ne v] 14.3 and 24.3 μm line luminosities are tightly correlated in a large sample of standard optically identified AGNs recently observed by *Spitzer* (Dudik et al. 2007), as can be seen in Figure 5. Employing a Spearman rank correlation analysis (Kendall & Stuart 1976) yields a correlation coefficient of $r_S = 0.97$ between the [Ne v] 14.3 and 24.3 μm line luminosities, with a probability of chance correlation of 6.7×10^{-12}, indicating a significant correlation. This relation implies similar densities of the [Ne v]-emitting gas in the galaxies in the sample. The best-fit linear relation yields

$$\log L_{[\mathrm{Ne\ v}]14} = 0.995 \log L_{[\mathrm{Ne\ v}]24} + 0.0566, \qquad (1)$$

with an rms scatter of 0.219 dex. We note that equation (1) is consistent with the relationship between the [Ne v] 14.3 and 24.3 μm line luminosities in standard AGNs observed by the *Infrared Space Observatory* (*ISO*; Sturm et al. 2002), as well as NGC 3367, the one galaxy in our current sample in which both lines were detected. The [Ne v]/[Ne II] line flux ratio for the 13 AGNs with both [Ne v] and [Ne II] detections by *ISO* ranges from 0.06 to 2.11, with a median value of 0.47 (Sturm et al. 2002). The [Ne v]/[Ne II] ratios for our seven galaxies range from approximately 0.01 to 0.27, with most falling below the lowest value observed in standard AGNs by *ISO*. The [O IV]/[Ne II] line flux ratio for the 17 *ISO* AGNs with both lines detected ranges from 0.15 to 8.33, with a median value of 1.73 (Sturm et al. 2002). The [O IV]/[Ne II] line flux ratios for our sample of seven galaxies range from 0.28 to 0.67, within the range observed in the nearby powerful AGN observed by *ISO*. For comparison, the few starburst galaxies that show detectable [O IV] emission have [O IV]/[Ne II] line flux ratios that range from 0.006 to 0.647 (median = 0.019; Verma et al. 2003) but show no [Ne v] emission.

We note that when mapping observations were used, line fluxes from SH and LH maps were extracted from identically sized apertures. However, because the LH slit is larger than the SH slit, fluxes obtained from the SH and LH modules for staring observations correspond to different extraction regions. The line ratios in this work, as well as those obtained from *ISO*, are subject to aperture effects and should be viewed with some caution. In particular, the emission from lower ionization potential species is likely to be more spatially extended than the emission from higher ionization potential species. Line flux ratios from both matched and nonuniform apertures with the SH and LH modules will therefore likely depend on the distance to the source.

Table 4 lists the [Ne v] 14 μm line luminosities for all seven of our galaxies. When we compile the line luminosities for the large (33) sample of optically identified standard AGNs with [Ne v] 14 μm detections recently observed by *Spitzer* from Dudik et al. (2007) and Gorjian et al. (2007), the [Ne v] 14 μm line luminosity ranges from $\sim 1 \times 10^{38}$ to $\sim 8 \times 10^{42}$ ergs s^{-1}, with a median value of $\sim 1 \times 10^{41}$ ergs s^{-1}. As expected for weak AGNs, the line luminosities for our candidate sample of AGN are significantly lower than those found for optically identified AGNs. Four out of the seven galaxies with [Ne v] detections have luminosities below the minimum value found in standard optically identified AGNs. Although NGC 4321, optically identified as a transition object, and NGC 3367 both have [Ne v] luminosities somewhat higher than the minimum value seen in standard AGNs, they are still both an order of magnitude less luminous than the median value observed in optically identified AGNs.

In Figure 6 we investigate the relationship between the [O III] λ5007 luminosity, for which extensive compilations are available in the literature, and the [Ne v] luminosity in our sample of galaxies compared with standard AGNs. The [O III] λ5007 emission is often assumed to originate primarily in gas ionized exclusively by the AGN and lying outside of the obscuring torus. Under these assumptions, it has been used as a measure of the intrinsic bolometric luminosity of the AGN (e.g., Heckman et al. 2004). As can be seen from Figure 6, there is a significant correlation between the [O III] and [Ne v] luminosities. Employing a Spearman rank correlation analysis for the standard AGN plotted in Figure 6 yields a correlation coefficient between the line luminosities of $r_S = 0.84$, with a probability of chance correlation

of 8×10^{-6}. The best-fit linear regression yields the following relation:

$$\log L_{[\mathrm{O\ III}]\ \lambda 5007} = 1.273 \log L_{[\mathrm{Ne\ V}]14} - 10.268. \quad (2)$$

The [Ne v] data for the "standard AGN" plotted in Figure 6 were compiled from Dudik et al. (2007), Weedman et al. (2005), Ogle et al. (2006), Gorjian et al. (2007), Haas et al. (2005), Cleary et al. (2007), and Armus et al. (2007). The standard AGNs are mostly Seyfert 1 galaxies, quasars, 3C radio galaxies, and a few bona fide Seyfert 2 galaxies, but all LINERs were excluded. The [O III] luminosities were taken from H97, Veilleux et al. (1997), and the extensive compilations of [O III] λ5007 emission-line data from Xu et al. (1999) and Whittle (1992). We note that none of the line luminosities plotted in Figure 6 are corrected for extinction.

There is considerable scatter in Figure 6 (rms scatter of 0.67 dex). This scatter is expected for a number of reasons. First, the [O III] fluxes used in Figure 6 were obtained using a wide range of apertures. Since [O III] emission can originate in both H II regions and the AGN narrow-line region, the luminosity can vary considerably with measurement aperture size and the distance to the galaxy. For example, [O III] λ5007 measurements were recently obtained by Moustakas & Kennicutt (2006) for two of the galaxies in our sample (NGC 4321 and NGC 4414). These observations show that the [O III] λ5007 nuclear ($2.5'' \times 2.5''$) flux is roughly 2 orders of magnitude lower than the flux integrated across the optical extent of the galaxy. Thus, the AGN's contribution to the total luminosity is variable in the sample. Since the high-ionization [Ne v] line is more sensitive to the AGN, having a negligible star formation component, variation in the [O III]/[Ne v] luminosity ratio with AGN strength is expected. Second, the [O III] luminosity is not corrected for extinction, and although the AGN contribution to the [O III] originates outside the torus, there still can be some extinction from the host galaxy, which is probably higher in our sample of galaxies, since they are late-type spirals. Figure 6 shows that the median [O III]/[Ne v] luminosity ratio in our sample of late-type galaxies is roughly 20 times less than the median value of the ratio for the standard AGN. Assuming a foreground screen geometry for the obscuring material, this difference in line flux ratio can be caused by an extinction of only $A_V \sim 3$ mag.

4.4. *Infrared Spectroscopic AGN Detection Rate*

Using infrared spectroscopy to identify AGNs, counting only the seven firm [Ne v] detections, the detection rate of AGNs in our sample of optically normal late-type galaxies is ~20%. However, the limited and variable signal-to-noise ratio of the observations leaves open the possibility that the detection rate could be higher if the sensitivity of the observations were uniform and higher. Figure 7 shows the distribution of detections as a function of the 3 σ [Ne v] 14 μm line sensitivity. Here galaxies are included in each bin if the 3 σ line sensitivity is equal to the value listed on the *X*-axis or better. Although our sample size is limited, precluding us from making statistically firm conclusions, Figure 7 suggests that the detection rate is not likely to be greater than ~30% even if deeper exposures were obtained in all the observations.

From the H97 sample, out of the full sample of 486 galaxies, 207 are of Hubble type Sbc and later, and only 16 (~8%) are optically classified as AGNs. Our infrared spectroscopic technique suggests that the AGN detection rate in optically normal late-type galaxies is ~30%, implying that the incidence of AGNs in late-type galaxies is possibly greater than a factor of 4 higher than what optical observations alone suggest.

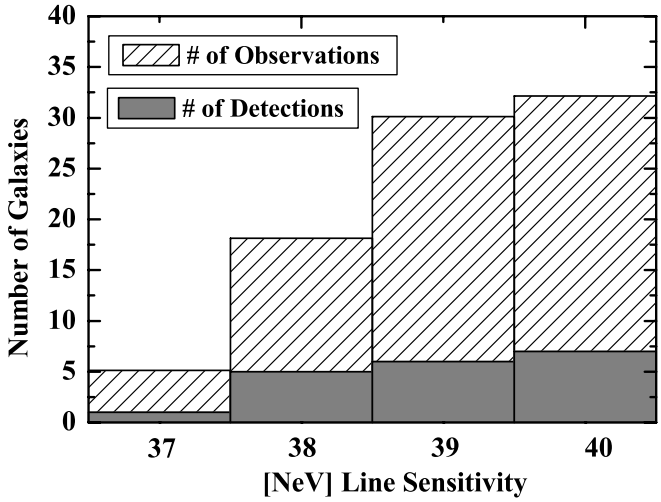

FIG. 7.—Distribution of galaxies with [Ne v] detections as a function of limiting line sensitivity. Plotted on the *X*-axis is the log of the 3 σ limiting [Ne v] 14 μm line sensitivity in units of ergs s^{-1}. Galaxies are included in each bin if the sensitivity of the observations is equal to or better than the value listed. Detections are indicated by the filled histogram. As can be seen, the detection rate at a limiting sensitivity of 10^{38} ergs s^{-1} is close to 30%.

Among the seven AGN candidates in our sample, three are Sbc galaxies, three are Sc galaxies, and one is of Hubble type Scd. Figure 1 shows the distribution of Hubble types for the sample with the seven AGN candidates indicated by the filled histogram. Since the sensitivity of the observations varied across the sample, we also indicate in Figure 1 (*arrows*) the number of galaxies with [Ne v] 14 μm 3 σ line sensitivity of 10^{38} ergs s^{-1} or better. Although the sample size is too small to make statistically firm statements, we note that none of the galaxies of Hubble type later than Scd display a [Ne v] line. Unfortunately, there are only three galaxies of Hubble type Sd. With such limited statistics it is not possible to say how common it is for Sd galaxies to host AGNs. A more extensive mid-infrared spectroscopic survey of Sd galaxies is crucial to obtain meaningful statistics on the number of completely bulgeless galaxies that contain accreting SMBHs.

5. AGN ORIGIN OF THE [Ne v] EMISSION

The detection of [Ne v] emission from the seven galaxies listed in Table 4 is highly suggestive of the presence of an AGN in these galaxies. In this section we summarize some of the published literature on each source, highlighting any previous evidence for nuclear activity. We also provide theoretical confirmation that the origin of the [Ne v] emission is indeed an AGN. Finally, we determine the contribution of the AGN to the total luminosity.

5.1. *Notes on Individual Galaxies*

NGC 3367.—NGC 3367 is an isolated face-on Sc barred galaxy (de Vaucouleurs et al. 1976) that is optically classified as an H II object. Its optical line ratios place it well to the left of the Kewley et al. (2001) starburst theoretical-limit line, as can be seen in Figure 1, indicating that there is no hint of the presence of an AGN from its optical spectrum. The aperture from which the [Ne v] 14.3 μm line was detected in this galaxy corresponds to a projected size of $\sim 1 \times 2.4$ kpc.

Although there is no hint of an AGN from optical observations, radio observations reveal a bipolar synchrotron outflow from a compact unresolved nucleus (of diameter less than 65 pc) and

possibly two large lobes straddling the nucleus that extend up to $\sim$12 kpc (García-Barreto et al. 1998). There are no *Chandra* or *XMM-Newton* observations of NGC 3367, but it was detected by *Einstein* (Fabbiano et al. 1992). The detection of the [Ne V] lines in this work firmly establishes the existence of a weak AGN in this galaxy. There are no published observations of the central stellar velocity dispersion in this galaxy.

NGC 3556.—NGC 3556 is an isolated edge-on Scd galaxy (de Vaucouleurs et al. 1976) that is also optically classified as an H II galaxy. As can be seen in Figure 1, its optical line ratios are at the extreme low end occupied by H II galaxies, well to the left of the starburst theoretical-limit line from Kewley et al. (2001). There is therefore absolutely no hint of the presence of an AGN in this galaxy in its optical spectrum. Adopting the distance to this galaxy from H97, the aperture from which the [Ne V] 14.3 μm line was detected corresponds to a projected size of $\sim 320 \times 770$ pc.

There are some previously published data that may be consistent with a weak AGN, as well as strong nuclear star formation in this galaxy. *Chandra* observations reveal numerous X-ray point sources scattered around the central regions, with one source coincident with the optical nucleus that has a power-law X-ray spectrum typical for an AGN (Wang et al. 2003). Prominent extraplanar diffuse X-ray emission is seen with substructure similar to that seen in Hα images (Collins et al. 2000) possibly representing superbubbles of hot gas heated in massive star-forming regions. There are no published observations of the central stellar velocity dispersion in this galaxy.

NGC 3938.—NGC 3938 is a nearly face-on Sc galaxy (de Vaucouleurs et al. 1976) at a distance of 17 Mpc (Tully & Shaya 1984) that is also optically classified as an H II galaxy. The [Ne V] 24.3 μm and [O IV] 26 μm lines were detected in this source in an $\sim 11'' \times 22''$ aperture which corresponds to a projected size of $\sim 0.9 \times 1.8$ kpc.

There are scattered H II regions in the central regions of this galaxy (Jiménez-Vicente et al. 1999) but no published evidence for AGN activity. The nucleus was undetected at 6 cm (Ulvestad & Ho 2002), and there are no published X-ray observations of this source. The central stellar velocity dispersion in this galaxy is 40 km s^{-1} (Bottema 1988).

NGC 4321.—NGC 4321 is an Sbc spiral galaxy (de Vaucouleurs et al. 1976) at a distance of 16.8 Mpc (Tully & Shaya 1984). At this distance, the aperture from which the [Ne V] 14.3 μm line was detected corresponds to a projected size of $\sim 0.9 \times 1.4$ kpc. This galaxy is optically classified as a transition object with no broad lines detected (H97), implying that there is no firm evidence for an AGN based solely only its optical spectrum.

Previously published multiwavelength observations reveal no signs of AGN activity in this galaxy. There are several published radio observations displaying extended emission (Filho et al. 2000, 2006), but no evidence for a compact flat spectrum radio core (Nagar et al. 2002). The nucleus is not detected by *Chandra*, and the upper limit to the 2–10 keV luminosity is $L_X \sim 3.6 \times 10^{38}$ ergs s^{-1} (Dudik et al. 2005), implying that the AGN is either weak or highly absorbed in the X-ray. Mid-infrared (Wozniak et al. 1998), optical (Pierce 1986), Hα (Knapen et al. 1995), and CO (Rand 1995) observations display a prominent circumnuclear ring of star formation activity which is also seen in the IRAC and [Ne II] images (see Fig. 4). However, the emission from the higher ionization potential [Ne III] and [O IV] lines is clearly centrally concentrated and compact, strongly suggestive of AGN activity in the nucleus. The central stellar velocity dispersion in this galaxy is 83 $\pm$ 12 km s^{-1} (Whitmore & Kirshner 1981).

NGC 4414.— NGC 4414 is a relatively isolated, flocculent Sc galaxy (de Vaucouleurs et al. 1976) that is optically classified as a transition object with no broad lines detected (H97). Therefore, there is no firm evidence for an AGN based solely on its optical spectrum. Its optical line ratios are very close to the Kewley et al. (2001) starburst theoretical-limit line, as can be seen in Figure 1.

There are no published observations of NGC 4414 suggesting that it contains an AGN. This source was not detected at radio frequencies by Filho et al. (2006), and arcsecond-resolution VLA observations reveal a diffuse radio morphology (Filho et al. 2000). There is also no indication of intense nuclear star formation. Based on its infrared and Hα luminosities, it is not classified as a starburst. In fact, Hα images show a central hole, indicating that there is no nuclear star formation (Pogge 1989) in this galaxy. Although there is no evidence for powerful star formation activity, H I and CO observations indicate that it has one of the highest disk neutral surface gas densities known (Braine et al. 1993). The central stellar velocity dispersion in this galaxy is 128 $\pm$ 9 km s^{-1} (Barth et al. 2002).

NGC 4536.—NGC 4536 is a barred late-type spiral (SABbc; de Vaucouleurs et al. 1976) that, based on *HST* imaging, shows no evidence of a classical bulge but instead has a surface brightness profile consistent with a pseudobulge that seems to exhibit spiral structure (Fisher 2006). This galaxy is optically classified by H97 as an H II galaxy. We detected the [Ne V] 14.3 μm line in this galaxy from an $\sim 580 \times 580$ pc region (adopting the distance to NGC 4536 from H97) approximately 10$''$ northeast of the optical nucleus of the galaxy. This is the only galaxy in our sample for which the [Ne V] emission seems to originate from a location that does not coincide with the optical nucleus as listed in the NASA/IPAC Extragalactic Database (NED). The [O IV] 26 μm and [Ne III] 15.5 μm emission, however, are centrally concentrated with a peak that is offset from the location of the [Ne V] emission and is closer to the optical nucleus than defined in NED, as can be seen from Figure 4. The [O IV] 26 μm line was not detected in the same aperture in which the [Ne V] 14.3 μm line was detected; the [O IV] flux is therefore listed as an upper limit in Tables 3 and 4 but is displayed in Figure 4. We note that the sensitivity of the current mapping observation of NGC 4536 is insufficient to conduct a full exploration of the spatial morphology of the [Ne V] emission in this galaxy. Deeper IRS mapping observations are critical to confirm the exact peak of the [Ne V] emission in this galaxy.

Apart from the [Ne V] detection reported in this work, to the best of our knowledge, there is only one previously published observation of NGC 4536 that hints at the possibility of nuclear activity in this galaxy. The optical line ratios obtained using recent high spatial resolution Space Telescope Imaging Spectrograph spectroscopy suggest the presence of a weak AGN (Hughes et al. 2005). There is abundant evidence for powerful nuclear star formation in NGC 4536. Its high far-infrared luminosity and strong Hα (Pogge 1989), Brγ (Puxley et al. 1988), and 10.8 μm (Telesco et al. 1993) emission suggest vigorous star formation in the central $\sim 20'' \times 30''$ region. The radio emission shows a diffuse morphology with three separate peaks (Vila et al. 1990; Laine et al. 2006), possibly representing an annular ring of star formation surrounding the nucleus. However, Laine et al. (2006) suggest, based on *HST* data, that the radio clumps are close to the nucleus in projection but that none correspond to the nucleus itself. This morphology is similar to that seen at 10.8 μm (Telesco et al. 1993), as well as in the 1–0 $S(1)$ molecular hydrogen line (Davies et al. 1997). We note that the variable resolution of most published observations, coupled with the fact that this galaxy is nearly edge-on and has an intricate central complex of emission at various wavelengths, makes it very difficult to confirm the spatial coincidence of the various sources.

The galaxy was detected by *Einstein* (Fabbiano et al. 1992). *ROSAT* High Resolution Imager data reveal two ultraluminous X-ray sources, one of which may be coincident with the optical nucleus (Liu & Bregman 2005). It is not possible, based on existing X-ray observations, to determine whether this source is consistent with an AGN. The galaxy was not observed by *Chandra*.

Our observations provide strong motivation to conduct an extensive high spatial resolution investigation at infrared and X-ray wavelengths of NGC 4536 to determine the exact location of the peak of the [Ne v] emission and to confirm its association with an AGN in this galaxy. The central stellar velocity dispersion in this galaxy is 84 ± 1 km s^{-1} (Batcheldor et al. 2005).

NGC 5055.—NGC 5055 is an Sbc spiral galaxy (de Vaucouleurs et al. 1976) at a distance of 7.2 Mpc (Pierce 1994). At this distance, the aperture from which the [Ne v] 14.3 μm line was detected corresponds to a projected size of $\sim 170 \times 380$ pc. This galaxy is optically classified as a transition object with no broad lines detected (H97). Hence, there is no firm evidence for an AGN based solely on its optical spectrum.

The evidence for AGN activity at other wavelengths is inconclusive. The nucleus is not detected at a number of radio frequencies, but it is detected at 57.5 MHz with a flux density of 2.1 Jy (Israel & Mahoney 1990), implying that the source is radio-quiet. A central UV source is detected; however, high-resolution *HST* observations show that it is resolved with a radius of $\sim$7 pc (Maoz et al. 1995) and shows no variability (Maoz et al. 2005). The UV emission from this galaxy is therefore most likely dominated by a nuclear star cluster. *Chandra* observations reveal the presence of numerous point sources scattered across the nuclear region and a bright, hard point source coincident with the optical and infrared nucleus (Flohic et al. 2006; Luo et al. 2007). Flohic et al. (2006) argue that the spectrum of this source is well-fitted by a two-temperature plasma model suggesting that the X-ray emission is powered by stellar processes. Conversely, Luo et al. (2007) report that the central source is well-fitted by an absorbed power law with a spectral index typical of an AGN. The [Ne v] detection reported in this work provides firm confirmation of an AGN in this galaxy. The central stellar velocity dispersion associated with the bulge in this galaxy is 103 ± 6 km s^{-1} (Heraudeau & Simien 1998.)

5.2. *Model Fits to the Mid-Infrared Fine-Structure Line Fluxes: The Power of the AGN*

The mid-infrared fine-structure line fluxes presented here can be modeled using photoionization models to confirm the AGN origin of the [Ne v] emission and, in principle, estimate the contribution of the AGN to the bolometric luminosities in the seven galaxies with [Ne v] detections. We use the spectral synthesis code CLOUDY (Ferland et al. 1998) to model the mid-infrared spectrum emitted by gas ionized by both an input AGN radiation field and a young starburst. The modeling, along with a more extensive exploration of parameter space, is described in detail by Abel & Satyapal (2008). In short, we assume a typical AGN radiation field with a continuum shape characterized by the standard UV bump and X-ray power law as given in Korista et al. (1997). The stellar continuum is chosen to be a 4 Myr continuous star formation model with a Salpeter initial mass function and star formation rate of 1 $M_{\odot}$ yr^{-1}, generated using the Starburst99 Web site (Leitherer et al. 1999). We have conservatively chosen to employ starburst parameters that generate the hardest ionizing radiation field. This selection results in the maximum contribution of the starburst to the high-ionization line fluxes. Our models assume a simple plane-parallel geometry with constant density typical of H II regions ($\log n = 2.5$ cm^{-3}). The ionization parameter U, the dimensionless ratio of ionizing flux to gas density, is varied, along with the percent of the contribution of the AGN to the total luminosity. The emission-line ratios are most sensitive to changes in these parameters. We emphasize that this is a simple model, presented here with the intent of illustrating the effect the AGN luminosity has on the infrared and optical line ratios and to show that the mid-infrared line fluxes for our sample of seven galaxies with [Ne v] detections cannot be explained by pure photoionization by a starburst, even when an extreme starburst spectral energy distribution (SED) is adopted.

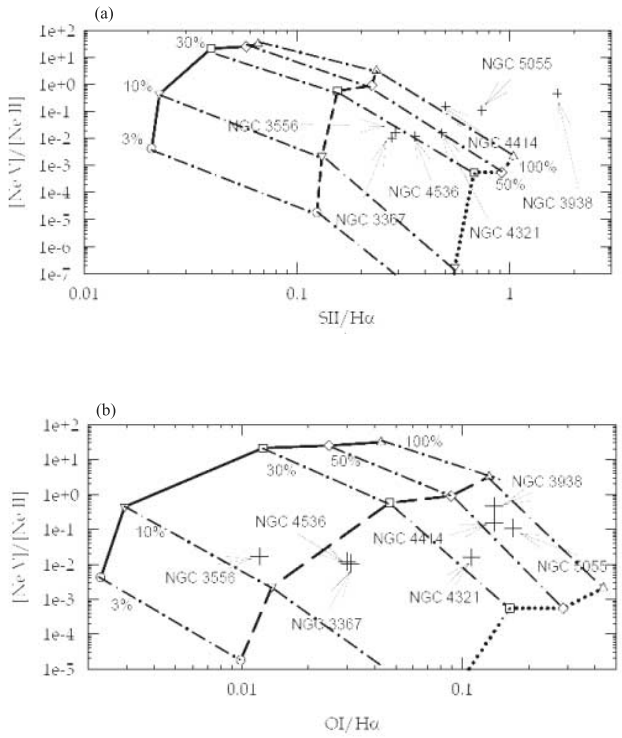

FIG. 8.—[Ne v] 14.3 μm/[Ne II] 12.8 μm line flux ratio vs. the optical (*a*) [S II]/Hα flux ratio and (*b*) [O I]/Hα flux ratio. The solid, dashed, and dotted lines display model results for ionization parameters of -1.5, -2.5, and -3.5, respectively. The dashed-dotted lines show the fraction of the total luminosity due to the AGN. The lines attached to the circles represent 3% AGN, inverted triangles 10% AGN, squares 30% AGN, diamonds 50% AGN, and triangles 100% AGN. The seven galaxies with [Ne v] detections are also displayed. We note that the optical line flux ratios are taken directly from Table 4 in H97.

Figure 8 shows the predicted [Ne v] 14.3 μm/[Ne II] 12.8 μm flux ratio versus the [O I]/Hα and [S II]/Hα optical line flux ratios for varying values of the U and AGN luminosity contribution, along with the observed values for all seven galaxies. We display only a narrow range of ionization parameters that generate line flux ratios within the range observed in our sample of galaxies. A more extensive grid of theoretical calculations, with all standard optical line flux ratios plotted, is presented in Abel & Satyapal (2008). As expected, Figure 8 shows that when the ionization parameter is held constant, the [Ne v] 14.3 μm/[Ne II] 12.8 μm flux ratio increases dramatically as the AGN luminosity fraction increases. Indeed, for $\log U = -2.5$, the [Ne v] 14.3 μm/[Ne II] 12.8 μm flux ratio increases by over 5 orders of magnitude as the AGN luminosity fraction increases from 3% to 100%. In contrast, the optical line flux ratios vary by only a factor of $\sim$10. Note that when the AGN luminosity fraction increases from 0.1% to 10%, *there is essentially no change in the optical line flux ratios*. Figure 8 clearly shows that *infrared diagnostic ratios are much more sensitive to weak AGNs than optical diagnostic ratios*. This regime of parameter space is clearly best explored using

the high-ionization mid-infrared emission-line fluxes presented in this work.

Surprisingly, when the AGN luminosity fraction goes to zero, [Ne v] emission is still produced exclusively by the starburst. The production of Ne^{4+} requires photons with energies >97 eV, not typically produced by hot O stars. However, an extremely young starburst with a large population of Wolf-Rayet and O stars can produce significant emission in the extreme UV (Schaerer & Stasińska 1999; see Abel & Satyapal [2008] for a more extensive discussion of this result). However, as can be seen from Figure 8, it is impossible to replicate the observed mid-infrared and optical line flux ratios in our sample of seven galaxies with purely a starburst ionization radiation field. An AGN contribution is required to explain the observed [Ne v] emission in all cases.

Figure 8 shows that three of the galaxies, NGC 3556, NGC 3367, and NGC 4536, appear to be dominated by star formation, while the other four galaxies likely have a more substantial contribution from an AGN. NGC 3556 could have as little as 10% of its luminosity coming from the AGN. The best-fit ionization parameter for our sample of galaxies lies between $\log U = -2.5$ and -3.5. The line flux ratios for NGC 4321 are consistent with a 30%–50% contribution from an AGN. From Figure 8 it is clear that NGC 5055, NGC 3938, and NGC 4414 are not well fit by our current model. The line ratios in these objects cannot be replicated by changing the AGN SED, model geometry, or starburst SED, indicating that it is likely that, in addition to photoionization by an AGN, shock excitation of the narrow-line region gas plays a significant role in these galaxies. Indeed, an examination of several of the standard optically identified AGNs with previously published mid-infrared spectroscopic observations (e.g., Sturm et al. 2002) shows that they too cannot be modeled solely using photoionization calculations, indicating that different physical mechanisms are at work in most AGNs. Clearly, further theoretical work studying the combined effects of shocks and photoionization is needed. In order to obtain a more precise estimate of the AGN fraction to the total luminosity, a model that includes the effects of shocks is required and will be explored in a future paper. In this paper we simply report that it is likely that NGC 4414, NGC 5055, and NGC 3938 have more dominant AGNs, but the actual fraction of total luminosity due to the AGNs in these galaxies is not well determined using our current models.

6. AGN BOLOMETRIC LUMINOSITIES AND BLACK HOLE MASS ESTIMATES

We can obtain order-of-magnitude estimates of the bolometric luminosity of the AGNs in the seven galaxies with [Ne v] detections using the [Ne v] line luminosity. The starburst contribution to the [Ne v] luminosity is negligible for our sample (Abel & Satyapal 2008). Assuming that the line emission arises exclusively from the AGN, we follow the procedure adopted by S07 to estimate the nuclear bolometric luminosity of the AGN. Using the tight correlation between the [Ne v] 14 μm line luminosity and the AGN bolometric luminosity found in a large sample of standard AGNs (eq. [1] in S07), we list in Table 5 the estimates of the AGN bolometric luminosity for the seven galaxies with [Ne v] detections. This estimate assumes that the relationship between the [Ne v] 14 μm line luminosity and the bolometric luminosity established in more luminous AGNs (see S07) extends to the lower [Ne v] luminosity range for our sample. The nuclear bolometric luminosities in our sample range from $\sim 3 \times 10^{41}$ to $\sim 2 \times 10^{43}$ ergs s^{-1}, with a median value of $\sim 9 \times 10^{41}$ ergs s^{-1}.

If we make the assumption that the AGN is radiating at the Eddington limit, we can obtain a lower mass limit to the mass of the black hole. In Table 5 we list the lower limits to the black hole mass based on the AGN bolometric luminosity estimates. The Eddington mass estimates in our sample range from $\sim 3 \times 10^3$ to $\sim 1.5 \times 10^5$ $M_\odot$, with a median value of $\sim 7 \times 10^3$ $M_\odot$.

TABLE 5
Black Hole Properties

Galaxy Name (1)	$\log L_{bol}$ (ergs s^{-1}) (2)	$\log M_{Edd}$ ($M_\odot$) (3)	σ (km s^{-1}) (4)	$\log M_{BH}$ ($M_\odot$) (5)
NGC 3367	43.29	5.19	...	7.84
NGC 3556	41.91	3.81	...	7.38
NGC 3938	42.36*	4.26	40	4.82
NGC 4321	42.82	4.72	83	6.36
NGC 4414	41.94*	3.84	128	7.28
NGC 4536	41.78	3.68	84	6.39
NGC 5055	41.51	3.41	103	6.82

Notes.—Col. (1): Common source names. Col. (2): Bolometric luminosity in ergs s^{-1} estimated from the [Ne v] 14 μm luminosity using eq. (1) from S07. For L_{bol} marked with an asterisk, [Ne v] 14 μm line luminosity is estimated using the [Ne v] 24 μm line luminosity. Col. (3): Eddington mass luminosity calculated using estimated bolometric luminosity for the AGN. Col. (4): Central stellar velocity dispersion (km s^{-1}). References are given for each galaxy in § 5.1. Col. (5): Estimate of black hole mass based on the stellar velocity dispersion when available (see Akritas & Bershady 1996 and Ferrarese 2004) or the bulge magnitude for NGC 3556 and NGC 3367.

In order to determine whether the lower mass limits derived for the black hole mass are incompatible with the M_{BH}-σ relation, assuming a linear extrapolation to the mass range of our sample, we also list in Table 5 the expected black hole masses using the published central stellar velocity dispersions, when available, for our sources. In the absence of published central stellar velocity dispersion measurements, we list in Table 5 the black hole masses expected using the bulge magnitude, assuming the updated calibration of the Magorrian relationship from Ferrarese & Ford (2005). Estimates for the bulge magnitude in these cases are taken directly from Table 11 of H97 and are crude estimates based on the morphological type of the galaxy and its total luminosity. In all cases, our lower mass limit is below the black hole mass estimate based on the M_{BH}-σ relation by a factor of $\sim$4 to 3 orders of magnitude, indicating that our results are not necessarily inconsistent with the M_{BH}-σ relation.

7. SUMMARY AND CONCLUSIONS

We conducted a mid-infrared spectroscopic investigation of 32 late-type (Hubble type Sbc or later) galaxies showing no definitive signatures of AGNs in their optical spectra in order to search for low-luminosity and/or embedded AGNs. The primary goal of our study was to determine whether AGNs in low-bulge environments are more common than once thought. Our high-resolution *Spitzer* spectroscopic observations reveal that the answer to this question is *yes*. Our main results are summarized as follows:

1. We detected the high-ionization [Ne v] 14.3 and/or 24.3 μm lines in seven late-type galaxies, providing strong evidence for AGNs in these galaxies.

2. We detected the high-excitation [O iv] 25.9 μm and [Ne iii] 15.5 μm lines in five out of the seven galaxies with [Ne v] emission. Although these lines can be excited in star-forming regions, our mapping observations (when available) suggest that the emission is centrally concentrated and likely to be dominated by the AGN.

3. Taking into account the range of sensitivities of our observations, our work suggests that the AGN detection rate based on

mid-infrared diagnostics in late-type optically normal galaxies can be as much as or more than ~30%. This detection rate implies that the overall fraction of late-type galaxies hosting AGNs is possibly more than 4 times larger than what optical spectroscopic observations alone suggest.

4. Several of the galaxies with [Ne v] detections have optical emission-line ratios in the extreme "starburst range," indicating that there is absolutely no hint of an AGN based on their optical spectra. Three out of the seven galaxies are classified based on their optical line ratios as "transition objects," but none show broad permitted optical lines.

5. Of the seven AGN candidates in our sample, three are Sbc, three are Sc, and one is of Hubble type Scd. Since there are only three galaxies of Hubble type Sd, our limited sample size precludes us from making any definitive conclusions about the incidence of AGNs in completely bulgeless galaxies. The lowest central stellar velocity dispersion among the galaxies with published measurements is 40 km s^{-1}.

6. We demonstrate using photoionization models with both an input AGN and an extreme UV–bright starburst ionizing radiation field that the observed mid-infrared line ratios in our seven AGN candidates cannot be replicated unless an AGN contribution is included. These models show that when the fraction of the total luminosity due to the AGN is low, the optical diagnostics are insensitive to the presence of the AGN. In this regime of parameter space, the mid-infrared diagnostics offer a powerful tool in uncovering AGNs missed by optical spectroscopy.

7. Three of the galaxies, NGC 3556, NGC 3367, and NGC 4536, appear to be dominated by star formation. NGC 3556 could have as little as 10% of its luminosity coming from the AGN. NGC 4321, NGC 5055, NGC 3938, and NGC 4414 likely have a more dominant contribution to their luminosity from the AGN in addition to having some contribution to their emission-line fluxes from shock-excited gas. All of the galaxies that H97 classifies as H II galaxies are well characterized by a low AGN contribution, while all the transition objects seem to require some shock component.

8. The AGN bolometric luminosities inferred using our [Ne v] line luminosities range from $\sim 3 \times 10^{41}$ to $\sim 2 \times 10^{43}$ ergs s^{-1}, with a median value of $\sim 9 \times 10^{41}$ ergs s^{-1}. Assuming that the AGN is radiating at the Eddington limit, this corresponds a lower mass limit for the black hole that ranges from $\sim 3 \times 10^3$ to as high as $\sim 1.5 \times 10^5\ M_\odot$. These lower mass limits, however, do not put a strain on the well-known relationship between the black hole mass and the host galaxy's stellar velocity dispersion established in predominantly early-type galaxies.

The *Spitzer* spectroscopic study presented here demonstrates that black holes do form and grow in low-bulge environments and that they are significantly more common than optical studies indicate. In order to truly determine how common SMBHs and AGN activity are in *completely* bulgeless galaxies, a more extensive study with *Spitzer* is crucial.

We are very thankful to Diana Marcu and Brian O'Halloran for their invaluable help in the data analysis and to Jackie Fischer, Mario Gliozzi, and Rita Sambruna for their enlightening and thoughtful comments. We are also very grateful to Kartik Sheth and Daniel Dale for very helpful support with our questions about calibration and to the *Spitzer* helpdesk for numerous emails in support of our data analysis questions. We are also very grateful for the helpful comments from the referee, which improved this paper. This research has made use of the NASA/IPAC Extragalactic Database (NED), which is operated by the Jet Propulsion Laboratory, California Institute of Technology, under contract with the National Aeronautics and Space Administration. S. S. gratefully acknowledges financial support from NASA grant NAG5-11432. N. A. gratefully acknowledges NSF grant 0094050 and 0607497. R. P. D. gratefully acknowledges financial support from the NASA Graduate Student Research Program. N. P. A. would like to acknowledge financial support through the National Science Foundation under grant 0094050, 0607497 to the University of Cincinnati.

REFERENCES

Abel, N. P., & Satyapal, S. 2008, ApJ, in press
Akritas, M. G., & Bershady, M. A. 1996, ApJ, 470, 706
Armus, L., et al. 2007, ApJ, 656, 148
Barth, A., Ho, L., & Sargent, W. 2002, AJ, 124, 2607
———. 2004, in ASP Conf. Ser. 311, AGN Physics with the Sloan Digital Sky Survey, ed. G. T. Richards & P. B. Hall (San Francisco: ASP), 91
Batcheldor, D., et al. 2005, ApJS, 160, 76
Bottema, R. 1988, A&A, 197, 105
Braine, J., Combes, F., & van Driel, W. 1993, A&A, 280, 451
Cleary, K., Lawrence, C., Marshall, J., Hao, L., & Meier, D. 2007, ApJ, 660, 117
Collins, J. A., Rand, R. J., Duric, N., & Walterbos, R. A. M. 2000, ApJ, 536, 645
Dale, D. A., et al. 2006, ApJ, 646, 161
Davies, R. I., Sugai, H., & Ward, M. J. 1997, MNRAS, 291, 314
de Vaucouleurs, G., de Vaucouleurs, A., & Corwin, H. G. 1976, Second Reference Catalogue of Bright Galaxies (Austin: Univ. Texas Press) (RC2)
Dudik, R. P., Satyapal, S., Gliozzi, M., & Sambruna, R. M. 2005, ApJ, 620, 113
Dudik, R. P., et al. 2007, ApJ, 664, 71
Fabbiano, G., Kim, D. W., & Trinchieri, G. 1992, ApJS, 80, 531
Ferland, G. J., et al. 1998, PASP, 110, 761
Ferrarese, L. 2004, in Supermassive Black Holes in the Distant Universe, ed. A. J. Barger (Dordrecht: Kluwer), 1
Ferrarese, L., & Ford, H. 2005, Space Sci. Rev., 116, 523
Ferrarese, L., & Merritt, D. 2000, ApJ, 539, L9
Filho, M. E., Barthel, P. D., & Ho, L. C. 2000, ApJS, 129, 93
———. 2006, A&A, 451, 71
Filippenko, A. V., & Ho, L. C. 2003, ApJ, 588, L13
Fisher, D. B. 2006, in ASP Conf. Ser. 352, New Horizons in Astronomy, ed. S. J. Kannappan (San Francisco: ASP), 237
Flohic, H., Eracleous, M., Chartas, G., Shields, J. C., & Moran, E. C. 2006, ApJ, 647, 140
García-Barreto, J. A., Rudnick, L., Franco, J., & Martos, M. 1998, AJ, 116, 111
Gebhardt, K., et al. 2000, ApJ, 539, L13
———. 2001, AJ, 122, 2469
Genzel, R., et al. 1998, ApJ, 498, 579
Gorjian, V., Cleary, K., Werner, M. W., & Lawrence, C. R. 2007, ApJ, 655, L73
Greene, J. C., & Ho, L. C. 2004, ApJ, 610, 722
———. 2007, ApJ, 670, 92
Haas, M., Siebenmorgen, R., Schulz, B., Krugel, E., & Chini, R. 2005, A&A, 442, L39
Heckman, T. M. 1980, A&A, 87, 152
Heckman, T. M., Kauffmann, G., Brinchmann, J., Charlot, S., Tremonti, C., & White, S. D. M. 2004, ApJ, 613, 109
Heraudeau, P., & Simien, F. 1998, A&AS, 133, 317
Higdon, S. J. U., et al. 2004, PASP, 116, 975
Ho, L. C., Filippenko, A. V., & Sargent, W. L. W. 1997, ApJS, 112, 315 (H97)
Houck, J. R., et al. 2004, ApJS, 154, 18
Hughes, M. A., et al. 2005, AJ, 130, 73
Israel, F. P., & Mahoney, M. J. 1990, ApJ, 352, 30
Jiménez-Vicente, J., Battaner, E., Rozas, M., Castañeda, H., & Porcel, C. 1999, A&A, 342, 417
Kauffmann, G., & Haehnelt, M. 2000, MNRAS, 311, 576
Kauffmann, G., et al. 2003, MNRAS, 346, 1055
Keel, W. C. 1983, ApJ, 269, 466
Kendall, M., & Stuart, A. 1976, The Advanced Theory of Statistics, Vol. 2 (New York: Macmillian)
Kennicutt, R. C., et al. 2003, PASP, 115, 928
Kewley, L. J., Dopita, M. A., Sutherland, R. S., Heisler, C. A., & Trevena, J. 2001, ApJ, 556, 121

Knapen, J. H., Beckman, J. E., Heller, C. H., Shlosman, I., & de Jong, R. S. 1995, ApJ, 454, 623
Korista, K., Ferland, G., & Baldwin, J. 1997, ApJ, 487, 555
Laine, S., Kotilainen, J. K., Reunanen, J., Ryder, S. D., & Beck, R. 2006, AJ, 131, 701
Leitherer, C., et al. 1999, ApJS, 123, 3
Liu, J. F., & Bregman, J. N. 2005, ApJS, 157, 59
Luo, B., et al. 2007, Chinese J. Astron. Astrophys., 7, 335
Maoz, D., Nagar, N. M., Falcke, H., & Wilson, A. S. 2005, ApJ, 625, 699
Maoz, D., et al. 1995, ApJ, 440, 91
Merritt, D., Ferrarese, L., & Joseph, C. L. 2001, Science, 293, 1116
Moustakas, J., & Kennicutt, R. C., Jr. 2006, ApJS, 164, 81
Nagar, N. M., Falcke, H., Wilson, A. S., & Ulvestad, J. S. 2002, A&A, 392, 53
Ogle, P., Whysong, D., & Antonucci, R. 2006, ApJ, 647, 161
Pierce, M. J. 1986, AJ, 92, 285
———. 1994, ApJ, 430, 53
Pogge, R. W. 1989, ApJ, 345, 730
Puxley, P. J., Hawarden, T. G., & Mountain, C. M. 1988, MNRAS, 231, 465
Rand, R. J. 1995, AJ, 109, 2444
Satyapal, S., Sambruna, R. M., & Dudik, R. 2004, A&A, 414, 825
Satyapal, S., Vega, D., Heckman, T., O'Halloran, B., & Dudik, R. 2007, ApJ, 663, L9 (S07)
Schaerer, D., & Stasińska, G. 1999, A&A, 345, L17
Silk, J., & Rees, M. J. 1998, A&A, 331, L1
Smith, J. D. T., et al. 2004, ApJS, 154, 199
Sturm, E., et al. 2002, A&A, 393, 821
Telesco, C. M., Dressel, L. L., & Wolstencroft, R. D. 1993, ApJ, 414, 120
Terlevich, R., Melnick, J., & Moles, M. 1987, in IAU Symp. 121, Observational Evidence of Activity in Galaxies, ed. E. E. Khachikian, K. J. Fricke, & J. Melnick (Dordrecht: Kluwer), 499
Tully, R. B., & Shaya, E. J. 1984, ApJ, 281, 31
Ulvestad, J. S., & Ho, L. C. 2002, ApJ, 581, 925
Veilleux, S., & Osterbrock, D. E. 1987, ApJS, 63, 295
Veilleux, S., Sanders, D. B., & Kim, D.-C. 1997, ApJ, 484, 92
Verma, A., et al. 2003, A&A, 403, 829
Vila, M. B., Pedlar, A., Davies, R. D., Hummel, E., & Axon, D. J. 1990, MNRAS, 242, 379
Wang, Q. D., Chaves, T., & Irwin, J. A. 2003, ApJ, 598, 969
Weedman, D. W., et al. 2005, ApJ, 633, 706
Whitmore, B. C., & Kirshner, R. P. 1981, ApJ, 250, 43
Whittle, M. 1992, ApJS, 79, 49
Wozniak, H., Friedli, D., Martinet, L., & Pfenniger, D. 1998, A&A, 330, L5
Xu, C., Livio, M., & Baum, S. 1999, AJ, 118, 1169